

Size dependency of CdSe for light harvesting in quantum dots solar cell using COMSOL Multiphysics

Mirza Basyir Rodhuan^{1, b)}, Rosmila Abdul-Kahar^{1, a)}, Hajar Najihah Mohd Yazid¹,
Amirah Nabilah Mohd Rapi¹, Nur Hidayu Baharin¹, and Nanang Burhan^{2, c)}

¹*Photonic Devices and Sensor Research Centre (PDSR), Faculty of Applied Sciences and Technology,
Universiti Tun Hussein Onn Malaysia, Educational Hub Pagoh, 84600 Muar, Johor, Malaysia.*

²*Mechanical Engineering Department, Faculty of Engineering
Universitas Singaperbangsa Karawang, Karawang, Indonesia*

^{a)}Corresponding author: rosmila@uthm.edu.my

^{b)}gw190032@siswa.uthm.edu.my

^{c)}nanang.burhan@ft.unsika.as.id

Submitted: November-December 2022, Revised: January 2023, Accepted: February 21, 2023

Abstract. A solar cell (SC) can increase its performance by applying a semiconductor nanoparticle into it, and the name became quantum dots solar cell (QDSC). A nanotube of titanium dioxide (TiO₂) with various sizes of cadmium selenide (CdSe) quantum dots (QDs) was designed and simulated using COMSOL Multiphysics. This study is to identify the size of CdSe QDs that can harvest more light energy at 550 nm of wavelength through electric field distribution simulation. Following the result for CdSe QD that harvested highest at 550 nm of diameter size 3.0 nm, which matched the result of previous research, further study was done to look at the absorption percentage of this size. With the different structures of amorphous silicon SC, the maximum absorption value was 50.664% at 657 nm of wavelength and will increase to 52.819 % at 617 nm of wavelength when the 3 nm diameter size of CdSe is inserted. The presence of a certain size CdSe within an SC structure does improved the performance of SC.

INTRODUCTION

In order to meet this world's needs, one of the initiatives is to increase the performance of solar cells. The quantum technologies and solid-state physics knowledge were enlarged and intercepted, leading to the development of the quantum dots (QD). One of the objectives was to research on crystalline nanoparticle that connected the light and matter [1]. The semiconductor behaviour and optical qualities are analogous to an atomic structure; consequently, QDs are artificial atoms [2, 3]. When compared to atomic emitters, the multi-body nature of QDs increased the strength of the light-matter interaction; thus, QDs can be used in solar cells, known as quantum dots solar cells (QDSC) [1]. This ability of QDSC allows for greater photon absorption and makes them highly wanted for use in solar energy applications. QDSC is inexpensive to grow in terms of fabrication and can offer better efficiencies than conventional solar cells, making them the world's demand [4].

The solar cell is described as being a photovoltaic system. It is an electrical device that generates electrical power from sunlight (solar energy). Photovoltaic stands for a photo, meaning "light", and voltaic is "electricity". The solar cell is a PN junction. It works while the incoming photons hit the cell and are absorbed by the junction. Suppose the photon has energy greater than or the same as the bandgap energy of the semiconductor. The photon will be absorbed and switch its power to an electron producing an electron-hole pair. This electron-hole pair can go with the flow via a built-in electric field inside the PN junction and contribute to the device's net current [5]. A QDSC is the generation molecular absorber of solar cells design that uses QDs as the photovoltaic material. The size of QDs is too tiny and smaller than the size of the Bohr exciton radius to perform better in optical absorption. Thus, QDSCs are more effective in optical absorption than dye sensitised solar cells (DSSCs) [6].

QDs in QDSC with tuneable bandgap qualities are determined by the size of the QDs used in third-generation solar cells, which promise high efficiency, absorption, and cheap cost [7 – 9]. Because QDs have a sizeable inherent dipole moment, which causes fast charge separation and may create three electrons per photon due to multiple exciton production processes (MEG), they can collect more solar spectrum with their tuneable bandgap [8, 10, 11].

CdSe belongs to group II-IV materials where its bulk bandgap ($E_g = 1.74$ eV) lies in the solar energy spectrum. The traits of the chemically deposited CdSe strongly rely on the growth condition by changing the deposition key parameters [12]. Short-band-gap semiconductors can absorb visible light energy in the entire visible region of the solar cell. Like CdSe, their electronic traits are related to the size and shape of the crystal. If the size of the crystal is small, then the bandgap is high and extra electricity is needed to stimulate the dot. Eventually, more energy is released when the crystal returns to its resting state [13].

In recent years, experimenters have examined nanostructure regions; however, specific formulations and theories have strayed since the theoretical method is insufficient [14]. Researchers utilised simulations to build and handle the experiment computationally to gather the data for the study, employing various tools and approaches [15]. Some researchers have recently indicated that experiments and simulations may be used to investigate QDs. This is because QDs have nanoscale dimensions [16]. Cartar [14] sparked the study by applying the Finite Element Method (FEM) as a solution to a model of QDs that relied on Maxwell's equation as a foundation. On the other hand, previous papers stated that the QDs had not been computationally summarised, implying that their characteristics had not been modelled [14, 16, 17].

This research combines a component of the third generation of solar cells, a monolayer spherical CdSe QD, with a basic second generation of solar cells, the amorphous silicon solar cell (aSiSC) model design. COMSOL Multiphysics software was utilised to run the simulation. The light absorptions and electric field intensity of the aSiSC and aSiQDSC models are measured in this work, and the benefits of using CdSe QD in the aSiSC model are determined. Aside from that, the goal of this research was to figure out the physics notion underlying the procedure and how it affected the optical qualities of the CdSe QDs. As a result, this model design promises environmentally benign and high-efficiency solar cells, and it will serve as a foundation for future research and production of solar cells.

MATERIALS AND METHODS

The materials and properties used in this study were based on the research conducted by Kongkanand [3]. The quantum dot solar cells and semiconductor nanocrystals were the light harvesters and were redesigned in Fig. 1. Cadmium selenide quantum dot, CdSe QD, was chosen as a primary material for the design as it can serve as sensitizers for QDSC in five different sizes (2.0 nm, 2.6 nm, 3.0 nm, 3.7 nm and 4.0 nm). Three CdSe QDs were arranged in a single vertical array and were surrounded by a 12 nm height and 4.0 nm diameter of titanium dioxide (TiO_2) nanotube. This nanorod structure then was sandwiched by 0.5 nm thickness and 25.0 nm² area of platinum (Pt) and indium tin oxide (ITO) electrodes, as shown in Fig. 2.

The study was continued by simulating another model design: the amorphous silicon solar cell (aSiSC) model, to investigate its peak of optical absorption for 200 nm to 1000 nm of wavelengths. The model was adapted from [18] as shown in Fig. 3, where 3 nm of width and length and the layers included were 10 nm aluminium (Al), 26 nm amorphous silicon (aSi), 5 nm indium tin oxide (ITO), and 5 nm air layer. Then, the model was modified by placing 3.0 nm of CdSe QD within the model and sandwiched by aSi and ITO layers to observe the increment in optical absorption and its peak shift and labelled as aSiSCQD.

The simulation tool used was FEM using COMSOL Multiphysics 5.5 software to inspect the optical absorption and electric field profiles. The mathematical models used in this study were Maxwell's equations, Fresnel's equation, and Beer-Lambert's law. The delta of electric field \mathbf{E} from Faraday's and Ampere's laws in the general equation of electromagnetic waves (EMW) of the time-varying displacement current equation given by [19]

$$\nabla \times \nabla \times \mathbf{E} = -\nabla^2 \mathbf{E} = \mu\epsilon \frac{\partial^2 \mathbf{E}}{\partial t^2} + \mu\sigma \frac{\partial \mathbf{E}}{\partial t} \quad (1)$$

where μ is the permeability of the material, ϵ is the permittivity of the material, σ is the electrical conductivity of the material, and t is the time. The product of equation (1) and $e^{i\omega t}$ gives EMW equations in the frequency domain that are generally used in the FEM, which equals to

$$\frac{\nabla^2 \mathbf{E}}{\mu_r} - k^2 \left(\epsilon_r - \frac{i\sigma}{\omega\epsilon_0} \right) \mathbf{E} = 0 \quad (2)$$

where μ_r is the material relative permeability, ϵ_r is the material relative permittivity, ϵ_0 is the material permittivity of free space, σ is the electrical conductivity of the material, ω is the angular frequency, and k is the wavenumber [20].

The EMW propagates through the different mediums and combines with boundary conditions yielding refraction and reflection within the models. The Fresnel's equation of the reflection R and transmission T coefficients for s and p polarisations are [21]

$$R_s = \frac{n_1 \cos \theta_i - n_2 \cos \theta_t}{n_1 \cos \theta_i + n_2 \cos \theta_t} \quad (3)$$

$$R_p = \frac{n_2 \cos \theta_i - n_1 \cos \theta_t}{n_1 \cos \theta_i + n_2 \cos \theta_t} \quad (4)$$

$$T_s = \frac{2n_1 \cos \theta_i}{n_1 \cos \theta_i + n_2 \cos \theta_t} \quad (5)$$

$$T_p = \frac{2n_1 \cos \theta_i}{n_1 \cos \theta_i + n_2 \cos \theta_t} \quad (6)$$

where R_s is TE reflection coefficient, R_p is TM reflection coefficient, T_s is TE transmission coefficient, T_p is TM transmission coefficient, θ_i is the incident angle, θ_t is transmitted angle, n_1 and n_2 is the first and second refractive index of the material, TE and TM are defined as transverse electric and magnetic waves propagation, respectively.

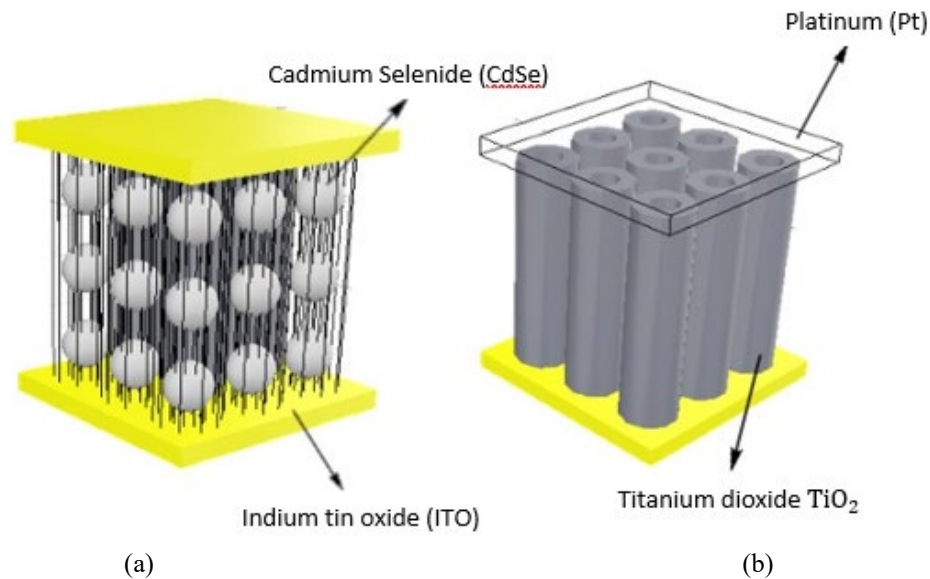


FIGURE 1. Complete design of quantum dot solar cell (QDSC) by Kongkanand [6].

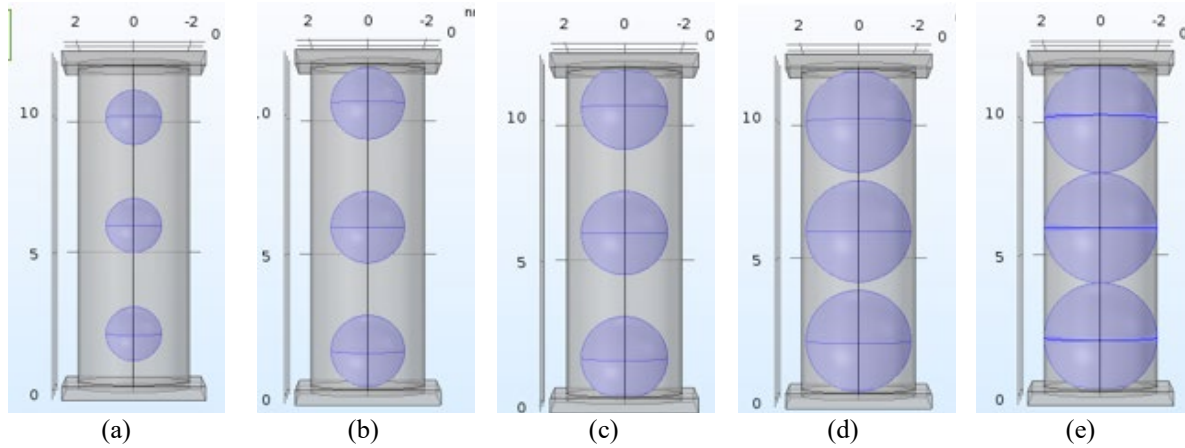


FIGURE 2. CdSe in a single column of TiO₂ nanotube with various size (a) 2.0nm (b) 2.6nm (c) 3.0nm (d) 3.7nm (e) 4.0nm sandwiched by Pt and ITO electrodes.



FIGURE 3. Amorphous silicon solar cell models (a) without CdSe QD and (b) with CdSe QD.

The incident EMW intensity I_0 propagates through the media and is scattered; thus, the transmitted EMW intensity I is observed to be lower than I_0 . This is because the properties of the model materials reduced the transmitted EMW, where some of it is being absorbed. By using Beer-Lambert's law, the absorption of EMW, A by the material can be obtained from equation (7) [22, 23]

$$A = \log_{10} \left(\frac{I_0}{I} \right) \quad (7)$$

where A is absorption. The good absorber materials give lower transmitted EMW intensity and vice versa.

RESULTS AND DISCUSSIONS

Figure 4 shows the 3.0 nm diameter of the CdSe QD has the most electric field that passes through the quantum dot solar cell. This is because the short-band gap semiconductor of 3.0 nm CdSe would harvest more light energy to the electrode surface. Another reason is that the size of the QDs is suitable and fit to put into QDSC. The quantisation of size allows tuning the visible response and the bandgap energy to modulate the charge transfer across different particles. The bandgap of 3.0 nm of particle CdSe able to initiate charge injection from excited Pt into ITO particle.

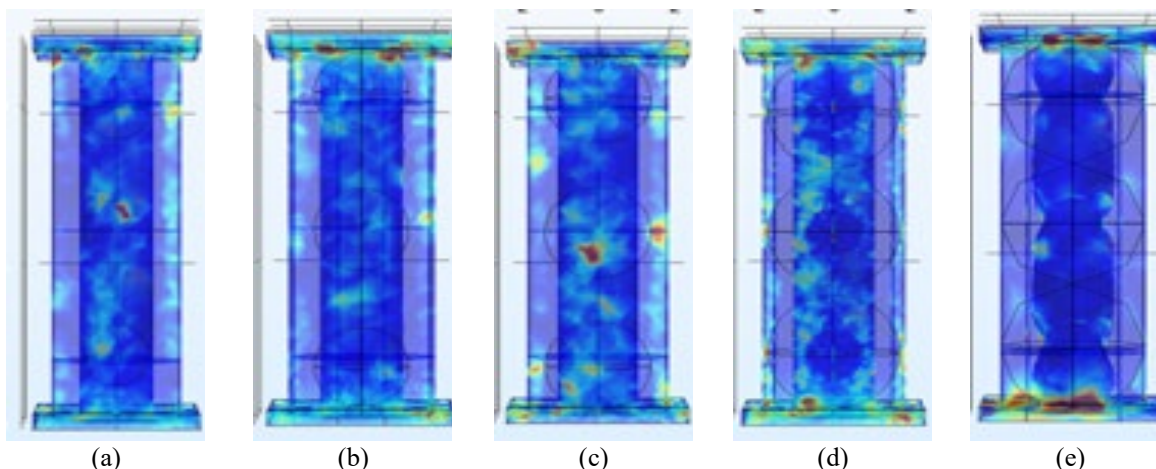


FIGURE 4. Electric field pattern when an electromagnetic wave of 550nm propagates into the QDSC with various size of CdSe

From the results, the lowest electric field distribution pattern was 3.7 nm due to its wide-bandgap semiconductor. In terms of colour, for all the simulations, the electric field in (E) was only on the outside which is on the counter electrode area (Pt and ITO). However, (B) and (D) resulted in a lower electric field distribution. This is due to the multiple reflections and resulting scattering on the interfaces between the nanoparticles. Although the resulting scattering is not that large compared to the other nanoparticles, it is still useful in producing more scattered photons. It can cause more energy conversion efficiency to be used in QDSC.

Based on the table 1, 3.0 nm performed the highest electric field value, which is 6.221456 V/m and 3.7 nm was the lowest, which is 5.887252 V/m. Next, the electric field for 2.0 nm, 2.6 nm and 4.0 nm were 5.981865 V/m, 5.955704 V/m and 6.003218 V/m, respectively. The results were matched with the result of Kongkanand [6] where 3.0 nm was the best diameter size to acquire the maximum IPCE (photon-to-charge carrier generation efficiency) and as SQ limit graph, but some error for some the 4.0 nm. Previous research showed that smaller particles demonstrate greater photoconversion efficiency but consume less light than larger particles. However, in this present study, from the simulations, the quantised particles have been successfully anchored on a nanorod array, so it should be possible to optimise the capture of incident light while increasing photoconversion efficiency.

The aSiSC and aSiSCQD models were designed and simulated. The optical absorption for both models was graphically shown in absorption percentage from 200 nm to 1000 nm of wavelengths, as shown in Fig. 5. It shows that the optical absorption curves were higher within the ultraviolet (UV) area (200 to 380 nm). This is because the energy of the EMW in the UV spectrum was more substantial than the material's bandgap. This results in the electrons' exciting from the valence band (VB) to the material's conductive band (CB).

From 380 nm to 1000 nm, the optical absorption eventually hiked within the visible spectrum and then decreased steadily to 1000 nm, near the infrared (NIR) spectrum. The optical absorption peaks in the visible spectrum happened as the frequency of light resonated with the natural frequency of the materials, consequently able to excite the electron from VB to CB. The materials were needily absorbed in the NIR spectrum due to the low energy of the EMW to make excitation of the electron as the frequency of light is larger than the natural frequency of the materials giving lower electronic transitions [24].

TABLE 1. Electric field (V/m) obtained with respect to the different diameter of CdSe from 2.0 nm to 4.0 nm.

Diameter of CdSe (nm)	Electric field (V/m)
2.0	5.981865
2.6	5.955704
3.0	6.221456
3.7	5.887252
4.0	6.003218

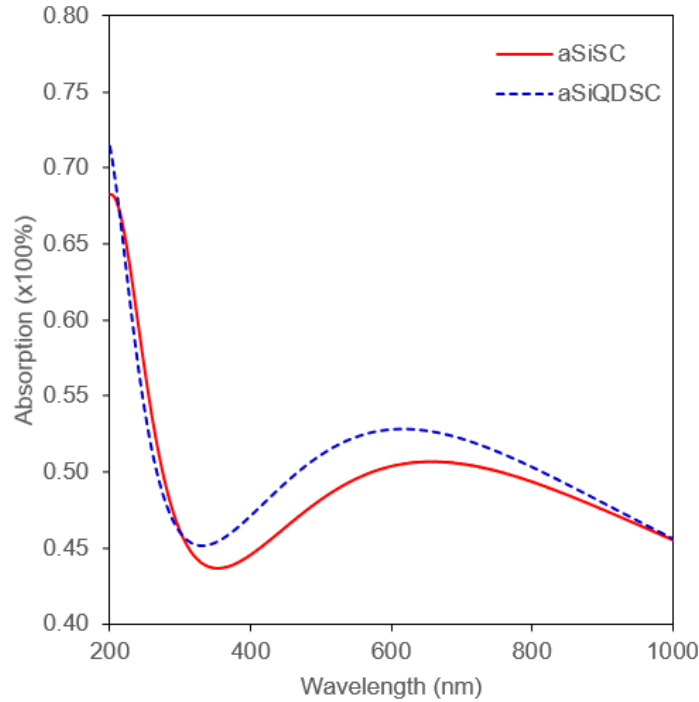


FIGURE 5. The optical absorption curves from 200 to 1000 nm by the aSiSC and aSiQDSC models.

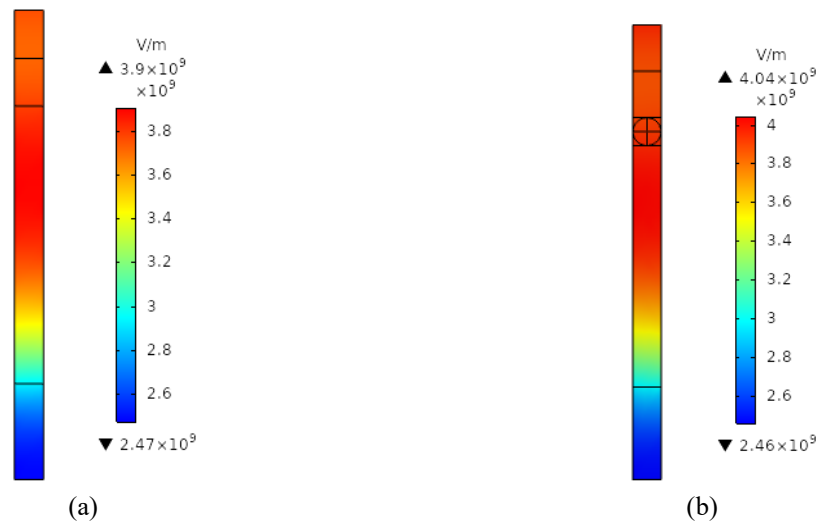


FIGURE 6. The electric field profiles within the entire (a) aSiSC, and (b) aSiQDSC models.

It has been detected the optical absorption peak by the aSiSC model was taken place in the wider wavelengths as the model was dominantly constructed by aSi where its optical absorption range was in the NIR spectrum [25, 26]. However, the optical absorption peak of the aSiQDSC model had higher than the aSiSC model. The peak was shifted, which occurred to the narrower wavelengths due to the quantum confinement effect within the QD and the optical absorption characteristics of the CdSe QD, respectively. Conferring to some previous experiments, the peak of optical

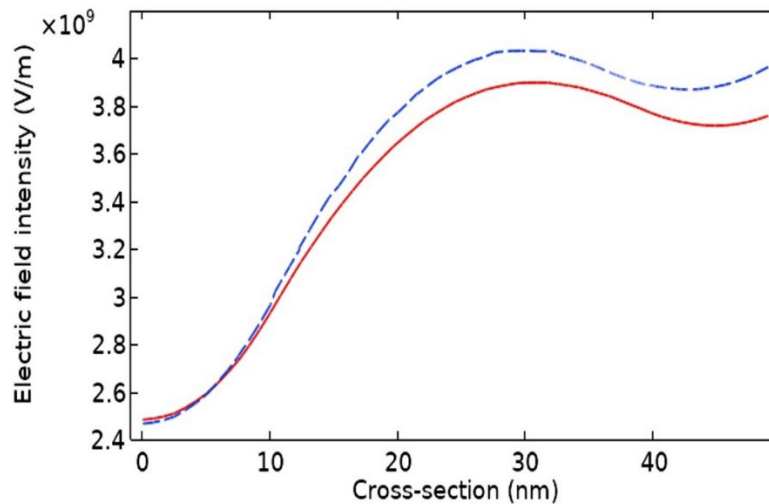


FIGURE 7. The cross-section electric field intensity within the entire (a) aSiSC (solid line), and (b) aSiQDSC models (dashed line).

absorption of the single CdSe QD was around 500 to 610 nm [26] and 513 to 562 nm [27]. These peaks shifted only in slight differences for both aSiSC and aSiQDSC models because of the massive presence of other materials within the models, which were predisposed to the entire optical absorption range curve. Strongly an optical absorption by the aSi, meanwhile, the size of CdSe QD and other materials were minor influences.

From the data obtained, the aSiSC model has 50.664% peak absorption, and the peak occurred at 657 nm, and for aSiQDSC model has 52.819% of peak absorption, which occurred at 617 nm. The existence of CdSe QD in aSiQDSC models yielded enhancement in optical absorption by 2.155% of increment compared to the aSiSC model.

The quantum confinement effect that leads to the multi-exciton generation (MEG) occurred within the CdSe QD and played a major role in enhancing optical absorption. In a bulk semiconductor, when the energy of the incident EMW is higher than the semiconductor bandgap, the electron can excite from VB to the higher level in the CB. The electron is known as a hot carrier electron as the hot carrier electron undergoes a bunch of nonradiative relaxations continually before going down to the lower level of CB.

On the other hand, the quantum confinement effect within the QD makes a large and discrete bandgap level in both VB and CB. Therefore, the hot carrier electron undergoes high light emission energy when relaxed to the lower level of CB. As the light emission has higher energy than the QD bandgap, it is absorbed by the next electron in the VB [28]. This phenomenon is known as MEG, where it only occurs within the QD. In a single incident energetic EMW can produce up to two or three electron-hole pairs, thus producing more energetic EMW when the recombination happens. In this process, there were a lot of energetic EMW from the incident, and CdSe QD then gave profits to the aSi in the aSiQDSC model compared to the aSiSC model, which only received incident energetic EMW.

Figure 6 shows the electric field distributions of the entire models for aSiSC and aSiQDSC models at their respective optical absorption peaks. At the nanoscale, the results clearly showed higher maximum electric fields recorded by the aSiQDSC model by 4.04 V/m, followed by aSiSC model by 3.9 V/m. These results also support the presence of CdSe QD in the models that have MEG making more electrons be excited within the model. Figure 7 depicts the cross-section electric field intensity of the entire aSiSC and aSiQDSC models at their respective absorption peak wavelengths. The curves show the aSi area had higher electric field intensity due to many exciting electrons being promoted in the aSi at the absorption peak. The results outlined that the aSiQDSC model has higher electric field intensity than the aSiSC model.

CONCLUSION

In summary, the various sizes of CdSe QDs in QDSC were successfully designed via COMSOL Multiphysics 5.5 with the certain parameters set and simulated by using Finite Element Method (FEM) to determine the perfect size of CdSe QDs that applied into a simple solar cell to harvest the light and also increasing the photoconversion

efficiency. The results showed that the 3.0 nm diameter of CdSe QD gave the highest electric fields compared to the other sizes. This concluded that 3.0 nm diameter of CdSe QD was the best size for harvesting 550 nm of incident light. The CdSe QD was then applied within another solar cell model, aSiSC to determine the enhancement effect of the optical absorption by the model. The peak of optical absorption by aSiSC and aSiQDSC models were 50.667% at 657 nm and 52.819% at 617 nm, respectively. The presence of CdSe QD within the SC model increases its optical absorption due to the quantum confinement effect that occurred within the QD, which leads to the MEG, which produces much energetic EMW to the aSi. Therefore, the presence of a certain size CdSe within an SC structure does improve the performance of SC.

ACKNOWLEDGEMENT

This study was supported by the Ministry of Higher Education (MOHE) through Fundamental Research Grant Scheme (FRGS) (FRGS/1/2019/STG02/UTHM/02/1) and Universiti Tun Hussein Onn Malaysia (UTHM) through vot K173.

REFERENCES

1. P. Tighineanu, "Electric and magnetic interaction between quantum dots and light," Ph.D. thesis, University of Copenhagen, 2015.
2. A. Delgado, M. Korkusinski, & P. Hawrylak, *Solid State Commun.* **305**, 113752 (2020).
3. T. K. Nideep, M. Ramya, and M. Kailasnath, *Superlattices Microstruct.* **130**, 175–181 (2019).
4. S. Sun, L. Gao, Y. Liu, and J. Sun, *Appl. Phys. Letters* **98**, 093112 (2011).
5. O. J. Woodford, "Photostability and the BOPHY architecture," Ph.D. thesis, Newcastle University, 2018.
6. A. Kongkanand, K. Tvrđy, K. Takechi, M. Kuno, and P. Kamat, *J. Am. Chem. Soc.* **130**, 4007–4015 (2008).
7. T. M. W. J. Bandara, and J. L. Ratnasekera, "Polymer Electrolytes for Quantum Dot-Sensitized Solar Cells (QDSSCs) and Challenges," in *Polymer Electrolytes: Characterization Techniques and Energy Applications*, edited by T. Winie, A. K. Arof, and S. Thomas (Wiley-VCH, Weinheim, 2020), pp. 299–337.
8. K. Surana, R. M. Mehra, and B. Bhattacharya, *Mater. Today: Proc.* **5**, 9108–9113 (2018).
9. P. Venkatachalam, and S. Rajalakshmi, *Mater. Today: Proc.* **22**, 400–403 (2019).
10. L. Hu, X. Geng, S. Singh, J. Shi, Y. Hu, S. Li, X. Guan, T. He, X. Li, Z. Cheng, R. Patterson, S. Huang, and T. Wu, *Nano Energy* **64**, 103922 (2019).
11. M. Xing, Y. Zhang, Q. Shen, and R. Wang, *J. Sol. Energy* **195**, 1–5 (2020).
12. K. Jasim, *KnE eng.* **3**, 171 (2018).
13. M. A. Hegazy and E. Borham, *NRIAG J. Astron. Geophys.* **7**, 27–33 (2018).
14. W. K. Cartar, "Theory and Modelling of Light-Matter Interactions in Photonics Crystal Cavity Systems Coupled to Quantum Dot Ensembles," Ph.D. thesis, Queen's University, 2017.
15. I. Richter, P. Kwiecien, and J. Ctyroky, "Advanced photonic and plasmonic waveguide nanostructures analysed with Fourier modal methods," in *2013 15th International Conference on Transparent Optical Networks* (Institute of Electronic and Electronics Engineers, Spain, 2013), pp. 1–7.
16. Y. Hong, Y. Wu, S. Wu, X. Wang, and J. Zhang, *Isr. J. Chem.* **59**, 661–672 (2019).
17. S. Zhai, P. Guo, J. Zheng, B. Suo, and Y. Wan, *Comput. Mater. Sci.* **148**, 149–156 (2018).
18. Z. Zhu, J. Sun, Z. Li, X. Yu, J. Zhao, and H. Dai, *Optik* **179**, 831–836 (2019).
19. F. Cheng, P. H. Su, J. Choi, S. Gwo, X. Li, and C. K. Shih, *ACS Nano* **10**, 9852–9860, (2016).
20. V. Giannini, X. Lu, N. P. Hylton, K. H. Lee, N. J. Ekins-Daukes, and S. A. Maier, "Solar cells with a multi-functional plasmonic light concentration layer," in *37th IEEE Photo-voltaic Specialists Conference* (IEEE, 2011), pp. 000864–000865.
21. O. Lehtikangas, T. Tarvainen, A. D. Kim, and S. R. Arridge, *J. Comput. Phys.* **282**, 345–359 (2015).
22. M. H. Muhammad, M. F. O. Hameed, and S. S. A. Obayya, "Absorption Enhancement in Hexagonal Plasmonic Solar Cell," in *Numerical Simulation of Optoelectronic Devices* (Institute of Electronic and Electronics Engineers, Spain, 2014), pp. 63–64.
23. M. Hu, J. Chen, Z. Y. Li, L. Au, G. V. Hartland, X. Li, M. Marquez, and Y. Xia, *Chem. Soc. Rev.* **35**, 1084–1094 (2016).
24. A. Shah, "Thin-Film Silicon Solar Cells," in *McEvoy's Handbook of Photovoltaics* (EPFL Press, Lausanne, 2018), pp. 235–307.

25. T. N. Truong, D. Yan, C. Samundsett, R. Basnet, M. Tebyetekerwa, L. Li, F. Kremer, A. Cuevas, D. Macdonald, and H. T. Nguyen, *ACS Appl. Mater. Interfaces* **11**, 5554–5560 (2019).
26. S. Prasad, H. S. AlHesseny, M. S. AlSalhi, D. Devaraj, and V. Masilamai, *Nanomaterials* **7**, 29 (2017).
27. B. M. Saidzhonov, V. F. Kozlovsky, V. B. Zaytsev, and R. B. Vasiliev, *J. Lumin.* **209**, 170–178 (2019).
28. K. Surana, R. M. Mehra, and B. Bhattacharya, *Mater. Today* **5**, 9108–9113 (2018).